

## Supporting Information

**Metallocelle Templated Transition Metal Nanostructures: Synthesis, characterization, DFT study and catalytic activity**

*Ravneet Kaur and S. K. Mehta\**

**Fig. s1** TEM image for Cu NPs at 4.5mM metal surfactant concentration (a) PAA capped, (c) bare; Enlarged image of Cu NPs (b) PAA capped, (d) bare.

**Fig. s2** EDX microanalysis for Cu NPs (a) PAA capped, (b) bare.

**Table s1** cmc values of metallosurfactants obtained by various techniques.

**Fig. s3** DLS curves for (a) Fe, (b) Co, (c) Ni, (d) Cu and (e) Zn metallomicelles at 4.5 mM concentration.

**Fig. s4** TEM image for Fe micelle at 4.5 mM concentration.

**Table s2** Optimised energy values for different NP systems (bare and ligand capped) using B3LYP-6-31G/LANL2DZ basis sets.

**Table s3** Vibrational assignment of various NPs.

**Fig. s5** UV-vis spectra for catalytic reduction reaction (a) without NPs, (b) in the presence of Cu metal (100 mesh size) with p-nitrophenol :  $\text{NaBH}_4 = 1:10$

**Fig. s6** UV-vis spectra for catalytic reduction reaction (a) without NPs, (b) in the presence of Cu metal (100 mesh size) with p-nitrophenol :  $\text{NaBH}_4 = 1:10$ . (All the catalytic reactions were monitored for 30 min with the aid of UV-vis spectroscopy and no significant change in spectra was observed after 30 -40 min.)

### Stability of bare and PAA capped metal NPs towards aerial oxidation

The NPs synthesized were evaluated for the stability towards air oxidation. For this purpose bare metal NPs synthesized by the above mentioned procedure and NPs with a protective PAA capping were analyzed and compared.<sup>1</sup> It was observed that the bare NPs got surface passivated in the presence of air and developed a layer of oxide on the surface while PAA protected NPs remained unchanged, which was confirmed using TEM and EDX studies. Figure S1 (a) & (b) is a representative TEM image obtained for PAA capped Cu NPs with metal surfactant: PAA molar ratio 1:0.5. The TEM image (dark and light fields) reveals polycrystalline nature of the Cu NPs formed, which is also evident from the enlarged view of Cu NPs showing different crystal planes. On the other hand, air-exposed bare Cu NPs show an internal void and shell–yolk type of structure (Figure S1 (c) & (d)) revealing the formation of oxide layer on the external surface. This type of behavior has already been observed for surface passivated NPs.<sup>2</sup> Enlarged clear TEM images could not be obtained for Fe as they are in QD regime while Co and Ni tend to show aggregate like structures and do not give clearly resolved TEM images.

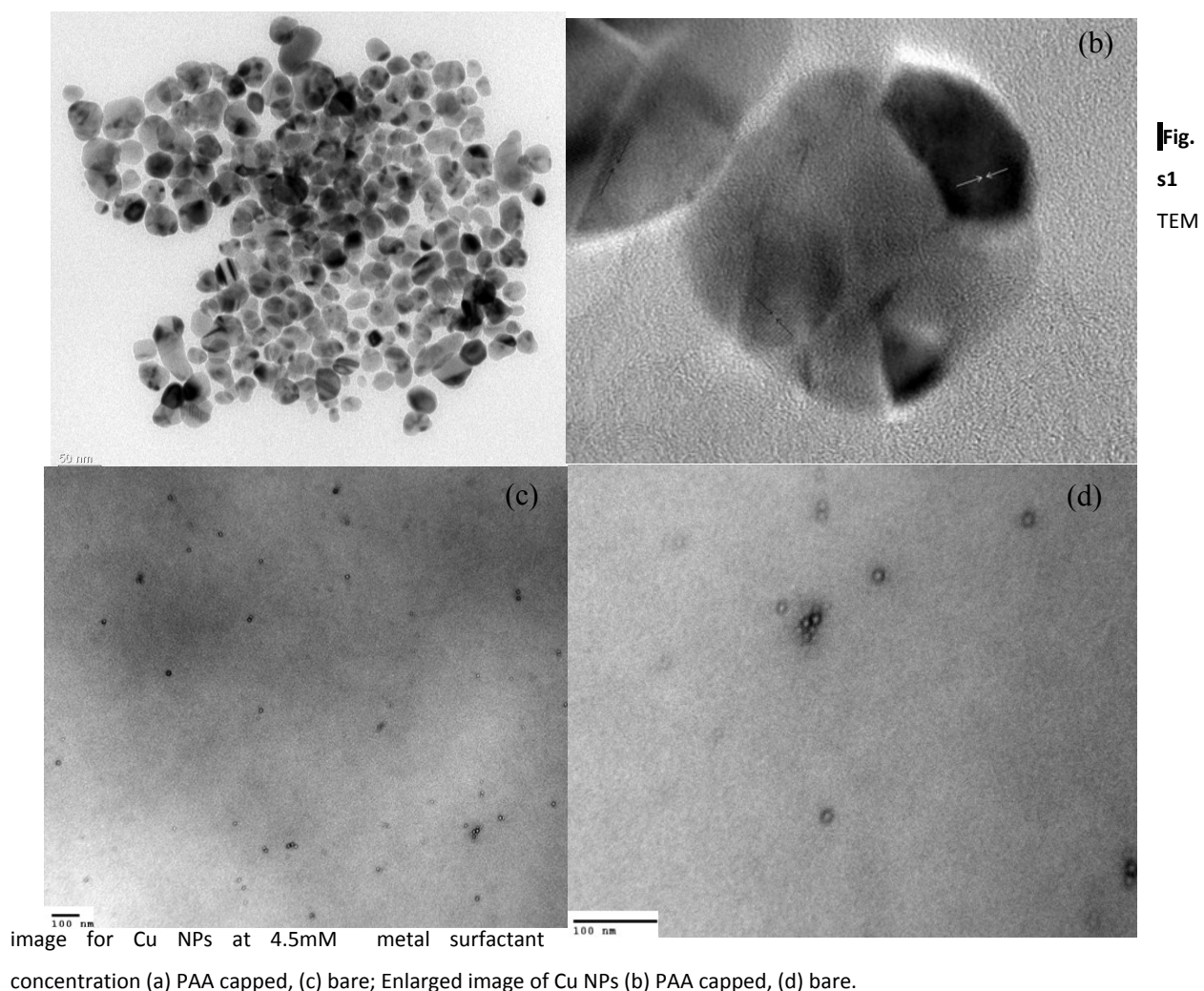
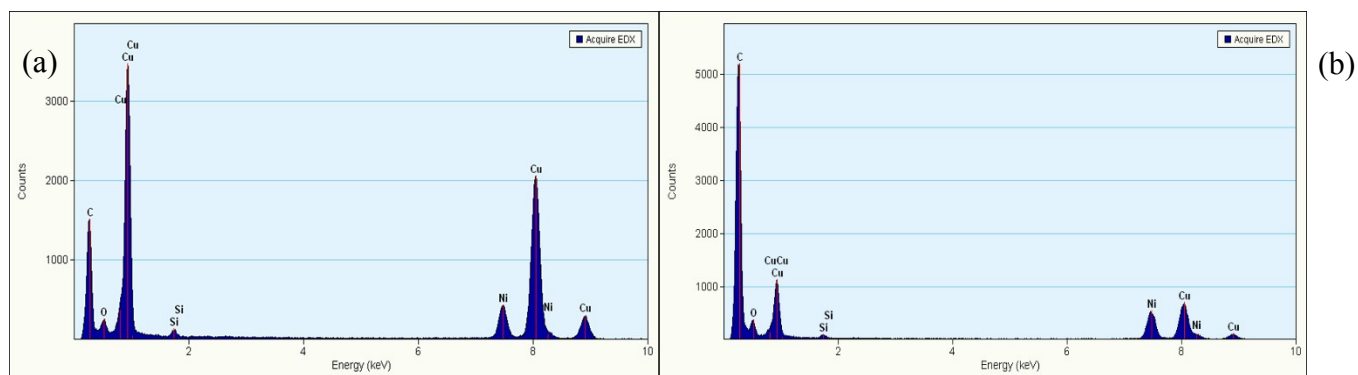


Fig. S1  
TEM

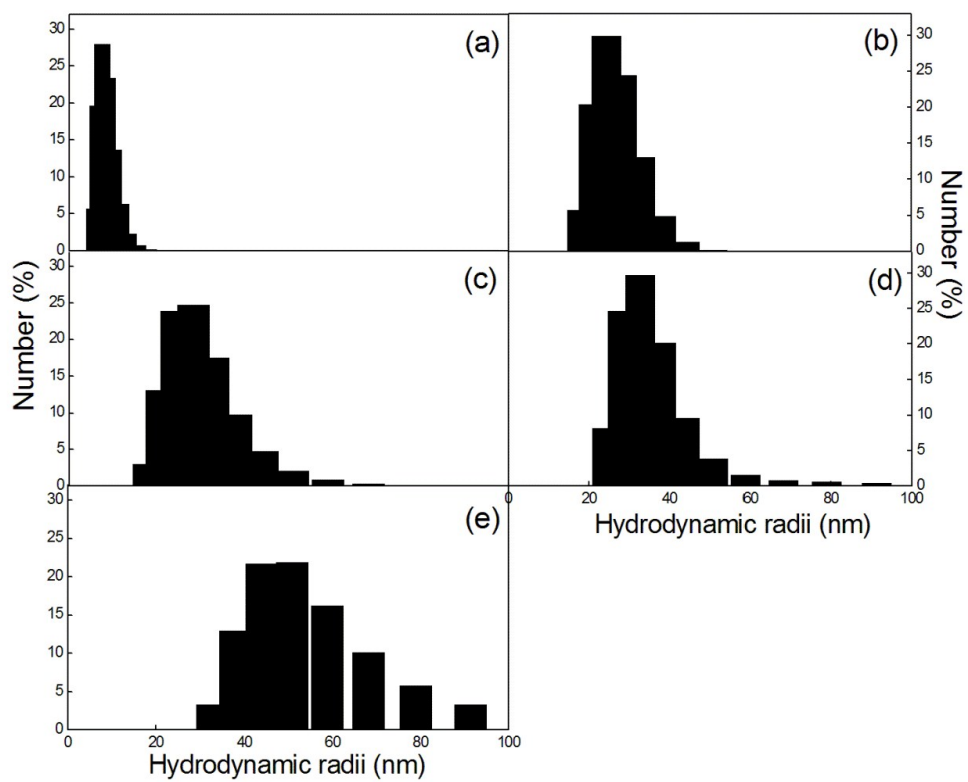
Energy-dispersive X-ray analyses of the particles were performed on a FEI Tecnai G<sup>2</sup> F20 electron microscope equipped with EDX detector, from Technische Universität, Germany. For the measurements, a drop of the nanoparticle solution was dispensed on a 3-mm carbon-coated copper grid. A formvar grid was not used as it contains additional C, H and O content. EDX studies used to analyze the components in the NPs confirmed the presence of an excess amount of oxygen in the unprotected/bare nanoparticle sample compared to the PAA capped sample (even in the presence of additional oxygen from acrylic acid group). EDX analysis using the same instrument have also been previously reported in literature, to determine the components present in alloys or core shell type of nanoparticles.<sup>[3]</sup> EDX microanalysis for the PAA capped Cu NPs show majority of peaks characteristic to copper. However, presence of trace amount of oxygen, may be attributed to the PAA or from water which is almost unavoidable (Figure s2 (a)). Compared to the PAA capped NPs, EDX spectrum for bare NPs shows a considerably higher amount of oxygen pointing towards oxide layer formation.



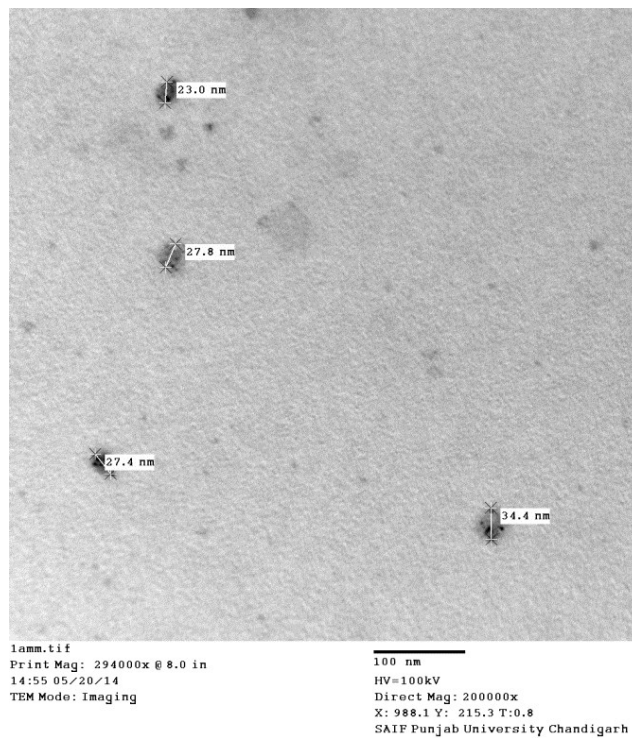
**Fig. s2** EDX microanalysis for Cu NPs (a) PAA capped, (b) bare.

**Table s1** cmc values of metallosurfactants obtained by various techniques.

Metallosurfactant	cmc/mM						
	CV	Density	Ultrasonic Velocity	Surface Tension	Conductivity	Adiabatic Compressibility	Literature value <sup>4</sup>
Fe	0.72±0.04	0.57±0.06	0.81±0.05	0.80±0.05	0.63±0.06	0.47±0.07	-
Co	0.95±0.05	0.96±0.06	0.77±0.05	0.85±0.08	0.89±0.04	0.77±0.05	0.90
Ni	1.23±0.05	0.82±0.05	1.02±0.06	1.30±0.08	0.89±0.04	0.79±0.06	-
Cu	0.82±0.06	0.77±0.04	0.90±0.06	0.91±0.07	0.84±0.05	0.81±0.05	0.90
Zn	0.28±0.06	0.69±0.06	0.57±0.08	0.25±0.04	0.34±0.05	0.47±0.05	-



**Fig. s3** DLS curves for (a) Fe, (b) Co, (c) Ni, (d) Cu and (e) Zn metallomicelles at 4.5 mM concentration.



**Fig. s4.** TEM image for Fe micelle at 4.5 mM concentration.


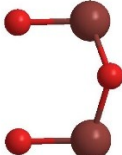




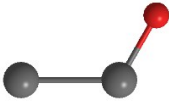

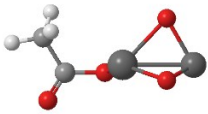

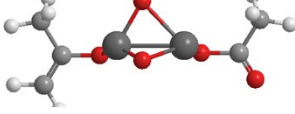
**Computational Details for choosing different basis sets (LANL2DZ and 6-31G):**

The computational models used here for simulation, have been previously cited in literature and chosen after extensive literature study to provide fairly good results especially for transition metal clusters, NPs, molecular complexes. They have been used by a number of research groups recently. Singh et al.<sup>5</sup> also reported that DFT with B3LYP hybrid functional, performed equally well as other correlated methods such as MP2 level of theory in predicting the molecular properties. Also, the interaction/binding energies observed are in the similar range as reported by various research groups. More recent examples of DFT-B3LYP/LANL2DZ and 6-31G basis sets especially in case of bare and ligand capped NPs are given below.

LANL2DZ basis set for the Au atom and 6-31+g(d, p) basis set for C, H, N and O atoms of curcumin molecule were chosen by Singh et al.<sup>5</sup> to study Au-curcumin interaction. It was reported that DFT with B3LYP hybrid functional, is superior to other two methods (Ab-initio and MP2). Kuznetsov et al.<sup>6</sup> also employed the first systematic DFT (B3LYP/LANL2DZ) to successfully study the structural (geometries and ligand binding energies) and electronic (HOMO/LUMO energy gaps,  $IP_{sv}$ , and  $EA_{sv}$ ) properties of  $Cd_nSe_n/Cd_nTe_n$  NPs ( $n = 6, 9$ ), for both bare and capped systems (with  $NH_3$ ,  $SCH_3$ , and  $OPH_3$  ligands). Chandraboss et al.<sup>1</sup> also carried out the experimental and first-principles study of guanine adsorption on ZnO clusters modeled by the B3LYP/ LANL2DZ method with different basis sets (B3LYP/6-31G, B3LYP/6-311G, MP2/6-31G and MP2/LANL2DZ) and reported that efficient binding could not be achieved by increasing the size of the clusters. Parsaee et al. also employed DFT calculations at the B3LYP levels of theory with a double basis set LANL2DZ for nickel, and a 6-31+G(d,p) basis set for the other atoms to model a novel nano-sized binuclear nickel(II) Schiff base complex as a precursor for NiO NPs.<sup>7</sup> DFT and TDDFT, was also used to investigate the effect of acetate groups on the electronic and optical properties of CdSe quantum dots (QDs). Optimizations were performed using the B3LYP hybrid functional and the mixed basis set LANL2DZ/6-31G\*, for Cd, Se and the atoms of the acetate.<sup>8</sup> The interactions between the capping ligands and ZnO surfaces were investigated by quantum chemistry calculation based on DFT by Chang and Waclawik.<sup>9</sup>

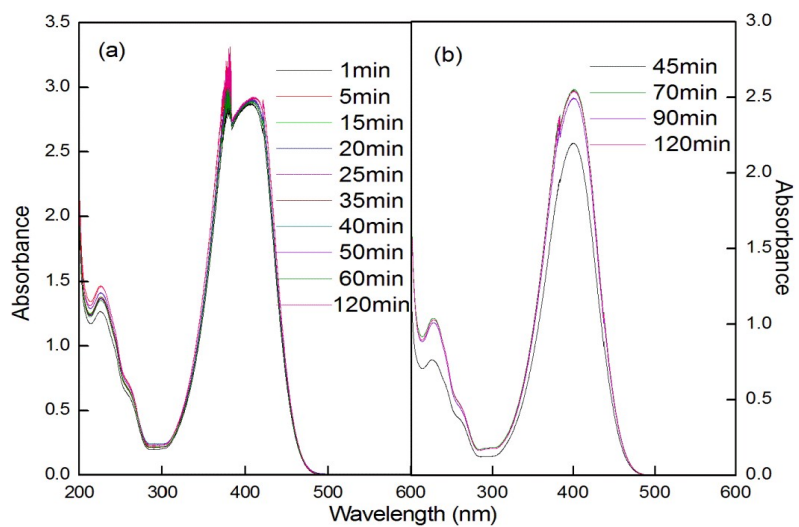


**Table s2** Optimised energy values for different NP systems (bare and ligand capped) using B3LYP-6-31G/LANL2DZ basis sets.

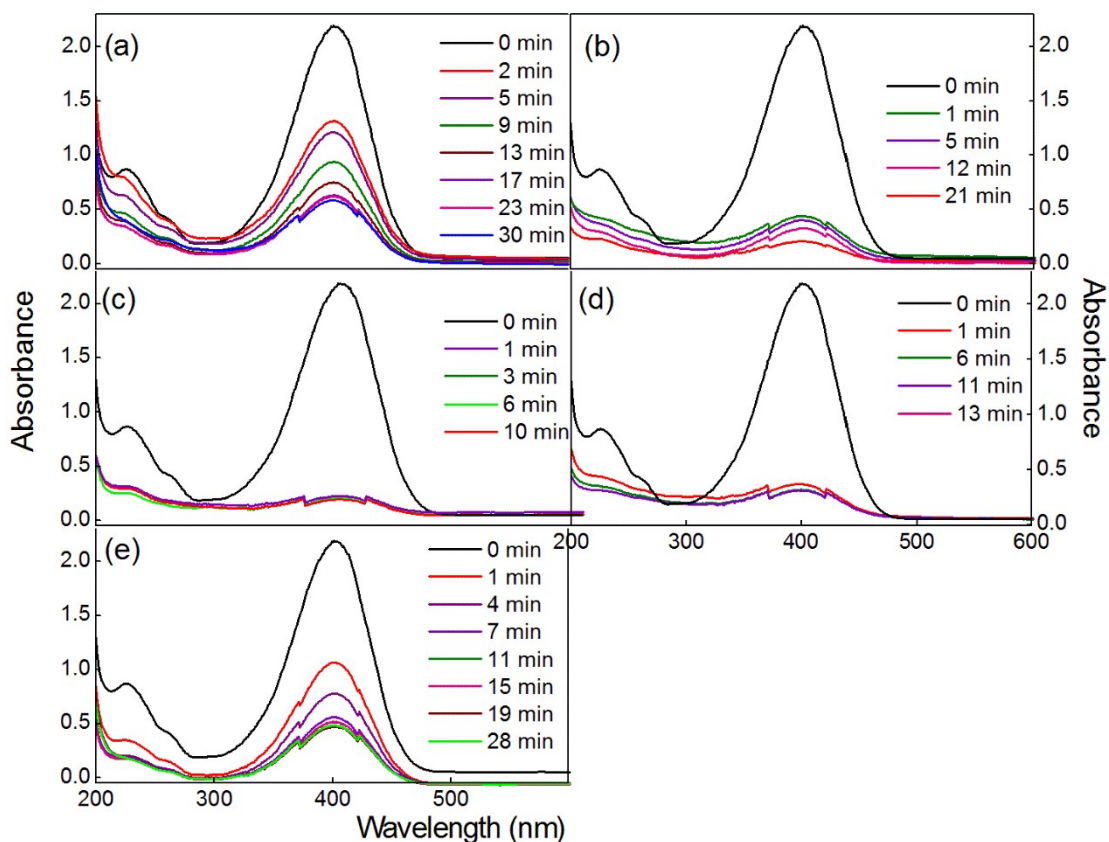
NP	Molecular Structures	$E_{NP}$ (a.u.) LANL2DZ	Molecular Structures	$E_{NP-L}$ (a.u.) LANL2DZ	$E_{NP}$ (a.u.) 6-31G
FeO		-198.41		-427.13	-1567.14
Fe <sub>2</sub> O <sub>3</sub>		-472.35		-824.17	-
CoO		-220.15		-748.50	-1985.92
NiO		-244.38		-772.70	-2114.78
CuO		-271.29		-791.82	-2243.63
ZnO		-140.71		-369.25	-2082.69
Zn <sub>2</sub> O		-206		-434	-3861.87
Zn <sub>2</sub> O <sub>2</sub>		-276.67		-510.19	-3937.04
Zn <sub>2</sub> O <sub>2</sub>		-276.67		-738	-

**Table s3** Comparison of the vibrational frequency values and vibrational assignment for various synthesized NPs; experimental data from FTIR and theoretical/computational data from DFT studies.

	Vibrational frequency values (cm <sup>-1</sup> )				
	Fe	Zn	Co	Ni	Cu
Vibrational frequency assignment	Experimental (theoretical)	Experimental (theoretical)	Experimental (theoretical)	Experimental (theoretical)	Experimental (theoretical)
$\nu_{\text{asymmetric}}(\text{COO}^-)$	1654 (1675)	1651 (1650)			
$\nu_{\text{symmetric}}(\text{COO}^-)$	1342 (1350)	1333 (1350)			
C-O stretching	1409 (1450)	1408 (1420)			
C-C stretching	996 (1050)	987 (1050)			
CH <sub>3</sub> rocking	1122 (1150)				
$\nu_{\text{asymmetric}}(\text{CH}_2)$			2910 (3100)	2917 (3100)	2918 (3100)
$\nu_{\text{symmetric}}(\text{CH}_2)$			2855 (2950)	2857 (3000)	2858 (2900)
NH <sub>2</sub> stretching			3344 (3450)	3377 (3500)	3355 (3400)
C-N stretching, CH <sub>3</sub> rocking			1100 (1150)	1080 (950)	1149 (1200)
C-H of CH <sub>3</sub>				1280 (1200)	



**Fig. s5** UV-vis spectra for catalytic reduction reaction (a) without NPs, (b) in the presence of Cu metal (100 mesh size) with p-nitrophenol :  $\text{NaBH}_4 = 1:10$



**Fig. S6** UV-vis spectra for catalytic reduction reaction (a) without NPs, (b) in the presence of Cu metal (100 mesh size) with p-nitrophenol :  $\text{NaBH}_4 = 1:10$ . (All the catalytic reactions were monitored for 30 min with the aid of UV-vis spectroscopy and no significant change in spectra was observed after 30-40 min.)

- 
- [1] R. Kaur, C. Giordano, M. Gradzielski, S. K. Mehta, *Chem.-Asian J.* **2014**, *9*, 189.  
 [2] G. Molteni, C. L. Bianchi, G. Marinoni, N. Santo, A. Ponti, *New J. Chem.* **2006**, *30*, 1137.  
 [3] J. Yang, E. H. Sargent, S. O. Kelley, J. Y. Ying, *Nature Mater.* **2009**, *8*, 683.  
 [4] A. M. Badawi, M. A. Mekawi, M. Z. Mohamed, M. M. Khowdairy, A. S. Mohamed, *J. Surfact. Deterg.* **2007**, *10*, 243-255.  
 [5] D. K. Singh, R. Jagannathan, P. Khandelwal, P. M. Abraham, P. Poddar, *Nanoscale*, 2013, *5*, 1882-1893.  
 [6] A. E. Kuznetsov, D. Balamurugan, S. S. Skourtis, D. N. Beratan, *J. Phys. Chem. C*, 2012, *116*, 6817-6830.  
 [7] Z. Parsaee, K. Mohammadi, M. Ghahramaninezhad B. Hosseinzadeh, *New J. Chem.*, 2016, *40*, 10569-10583  
 [8] P. K. Tamukong, W. D. N. Peiris, S. Kilina, *Phys. Chem. Chem. Phys.*, 2016, *18*, 20499-20510  
 [9] J. Chang, E. R. Waclawik, *J. Nano. Res.*, 2012, *8*, 1-12